Predicting the dynamic material constants of Mooney-Rivlin model in broad frequency range for elastomeric components

Abstract

In this paper, dynamic material constants of 2-parameter Mooney-Rivlin model for elastomeric components are identified in broad frequency range. To consider more practical case, an elastomeric engine mount is used as the case study. Finite element model updating technique using Radial Basis Function neural networks is implemented to predict the dynamic material constants. Material constants of 2-parameter Mooney-Rivlin model are obtained by curve fitting on uni-axial stress-strain curve. The initial estimations of the material constants are achieved by using uni-axial tension test data. To ensure of the consistency of dynamic response of a real component, frequency response function of three similar engine mounts are extracted from experimental modal data and average of them used in the procedure. The results showed that this technique can successfully predict dynamic material constants of Mooney-Rivlin model for elastomeric components.

Kamal Jahani [a]
Hossein Mahmoodzade [b]

[a] Mechanical Engineering Department, University of Tabriz , 29th Bahman Blvd., 51666-16471, Tabriz, Iran (phone: +98 411 3393044; fax: +98 411 3354153;
ka_jahani@tabrizu.ac.ir
[b] Mechanical Engineering Department, University of Tabriz , 29th Bahman Blvd., 51666-16471, Tabriz, Iran
h.mahmoodzade@gmail.com

1 INTRODUCTION

Elastomeric materials are widely used in noise and vibration isolation mechanisms at different industries such as automotive, aerospace, building and so on. Substantial improvement in isolator performance requires the construction of large quantity of samples and experimental tests that is very time consuming process. Proper use of finite element models can reduce the number of samples and experimental tests. Comparing metallic components, the mechanical properties of elastomers

are not well known and depend on many ambient and working conditions such as temperature, frequency and dynamic amplitude, etc (Rendek and Lion, 2010, Hofer and Lion, 2009). Therefore, using appropriate models for elastomers with proper material constants to achieve more realistic and accurate results is crucial in any finite element code. There exist some constitutive models (such as Mooney-Rivlin, Ogden, Neo-Hookean, Polynomial Form, Arruda-Boyce, Yeoh,...) that can simulate hyperelastic behavior of the elastomers. The Mooney-Rivlin constitutive model will be discussed in more details in this paper.

Usually elastomeric components experience both shock loads (that exert large deformations on the elastomer in low frequency) and vibration loads (that excite the component in low amplitude deformation and high frequency). In most of the published works, the static (or low frequency) tension /or compression tests have been conducted on the samples and using curve-fitting techniques, the material constants of Mooney-Rivlin model have been extracted. Guo and Sluys (2006) discussed different static tension test methods to extract the material constants and used these results to verify their proposed constitutive model. Cristopherson and Jazar (2006) used Mooney-Rivlin model in FE modeling of a passive hydraulic engine mount and determined the Mooney-Rivlin constants by curve fitting on uniaxial experimental stress-strain data. Khalilollahi *et al.* (2002) investigated the static behavior of elastic materials using Mooney-Rivlin model. The material coefficients of the model were achieved using experimental tests. Silva and Bittencourt (2008) used Mooney-Rivlin hyperelastic model in shape optimization of elastomeric media of an engine mount. Pereira and Bittencourt (2010) used the 2 parameter Mooney-Rivlin constitutive model in topological sensitivity analysis. Pearson and Pickering (2001) obtained the constants of Mooney-Rivlin model using axial tensile test and showed that using these constants, the static behavior of the elastomeric material is predicted well. Korochkina *et al.* (2008) investigated the applicability of various constitutive models to predict the nonlinear stress–strain behavior of silicone rubber pads. To determine the material parameters, they used uni-axial tension and pure shear test data. The material parameters were determined through a least-squares-fit procedure, which minimizes the relative error in stress.

To determine the dynamic mechanical characteristics of elastomers, in most of the documented methods the elastic and storage moduli (or elastic modulus and loss factor) have been used as material properties where, these properties extracted from resonant tests (Gupta *et al.*, 1999, Jahani and Nobari, 2010, Wismer and Gade, 1997). However, there are a few publications about dynamic material constants of the hyperelastic models for elastomers at broad frequency range. For instance, Kim *et al.* (2004) formulated a new constitutive model by using Mooney-Rivlin constants to predict the dynamic characteristic of rubbers superimposed to large static deformation but, they only presented results for frequencies below 30 Hz.

In the present paper, dynamic material constants of 2-parameter Mooney-Rivlin model for an elastomeric engine mount are identified in the broad frequency range. At first, the correctness of the model in predicting the non linear force-displacement relationship of the component is shown through comparing the results of static test and finite element model. Radial Basis Function Neural Networks method (RBFNN) is implemented to derive the dynamic material parameters from FE and experimental modal data. Frequency response function data of the updated 3-D FE model are used as training sets in identification process.

2 EXPERIMENTS AND TEST SAMPLES

2.1 Samples

To consider a more practical case in the present work, an elastomeric engine mount is investigated that is illustrated in Figure 1. The component includes upper and lower steel brackets and elastomeric media in the middle. The engine mount is a flat type and elastomeric media approximately has cubic shape.
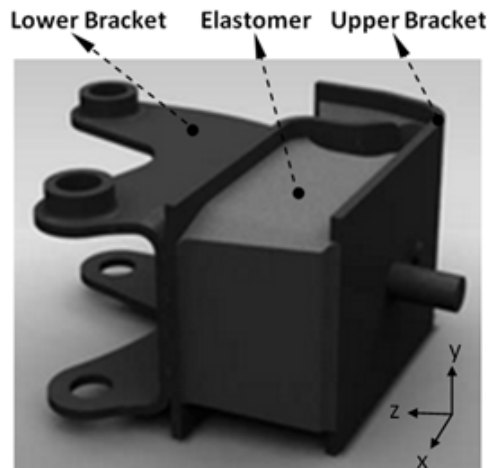

Figure 1: Investigated elastomeric engine mount.

2.2 Tests

2.2.1 Tension Test

To obtain Mooney-Rivlin constants, present method rely only on the 3-D FE model of the elastomeric sample and experimental FRF(Frequency response function) data and is independent of experimental stress-strain curves , however to have initial estimation of Mooney-Rivlin constants, the sample was stretched in the vertical direction(z-direction). Using the graph of stress-strain obtained from tension test and implementing curve fitting, the initial static coefficients of the material model were obtained. A schematic of tensile test rig is presented in Figure 2. The stress-strain graph of the investigated sample and curve fitted graph have been shown in Figure 3. Mooney-Rivlin material constants for the investigated engine mount that extracted from curve fitting procedure are: $c_{10}^0 = 2621676$ and $c_{01}^0 = -1851093$ (brief explanations of these material constants are presented in section 3.2).
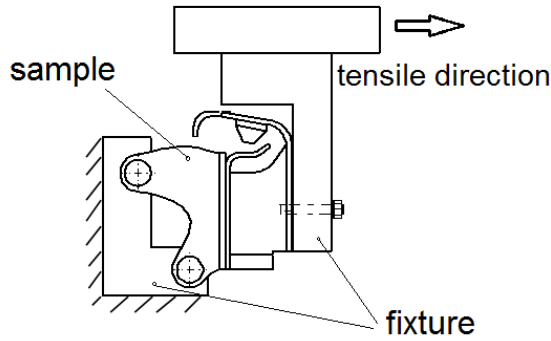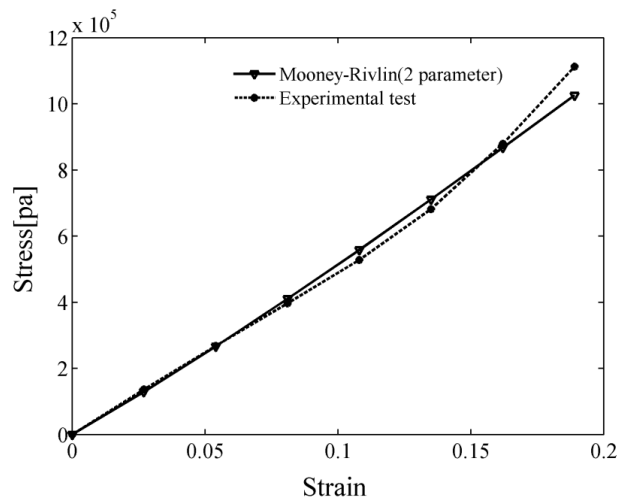
Figure 2: Schematic of tensile test rig.

Figure 3: The stress-strain graph of the sample and fitted graph.

2.2.2 Modal tests of the samples

Experimental FRF data of the engine mount is obtained by impact hammer test and modal analysis. A schematic of the modal test train is presented in Figure 4. Specifications of Test tools and instruments used in this study are presented in Table 1. Tests are done in vertical or z- direction in free-free condition. Atmospheric conditions of the lab during the tests were as following: Relative humidity=50%; Temperature=26°C. In order to ensure of the reliability and repeatability of the test results, 3 similar samples are tested. For instance, FRFs of the samples in z-direction are plotted with together in Figure 5. The natural frequencies of three samples are presented In Table 2.

Item	Mark and Type
Data logger and signal analyzer unit	B&K 2035
Impact hammer	B&K 8202
Accelerometer	B&K 4395
Tension test machine	MTS

Table 1: Test tools and instruments.

Natural Frequency (Hz)		
Sample1	Sample2	Sample3
212	193	192
394	381	379
576	576	570
762	702	691

Table 2: Natural frequencies of the engine mounts in vertical (z) direction in free-free condition.
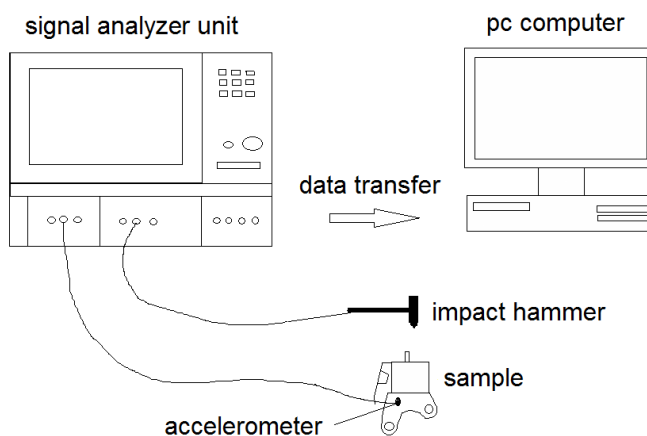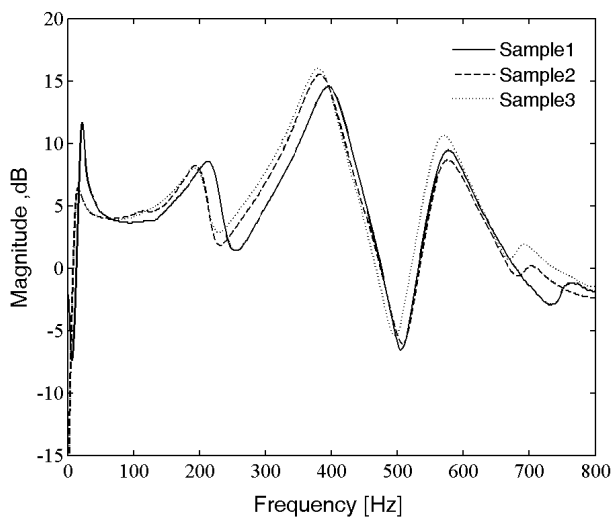

Figure 4: Schematic of Modal test train.

Figure 5: FRFs of the samples in z-direction.

2.2.3 Modal test of metallic parts of the sample.

Each of the samples has two metallic parts namely lower bracket assembly and upper bracket assembly. For the purpose of model updating task (see section 3.1.), the brackets of one of the investigated engine mounts separated from elastomeric part and cleaned then FRFs of these metallic parts are obtained using impact hammer test in free-free condition. In Table 3, the natural frequencies of the brackets are presented.

	Natural frequencies [Hz]		
	z- direction	y-direction	
Upper bracket	540	-	
Lower bracket	636	293	504

Table 3: Natural frequencies of the investigated engine mount's brackets in z-direction.
.

3 FE MODEL

The brackets are modeled using shell elements (shell 281) and elastomeric media is modeled using 3-D solid elements (8 nodes brick elements namely solid185) and 2- parameter Mooney-Rivlin model is selected as the material model in Ansys software. FE model of the sample is illustrated in Figure 6.
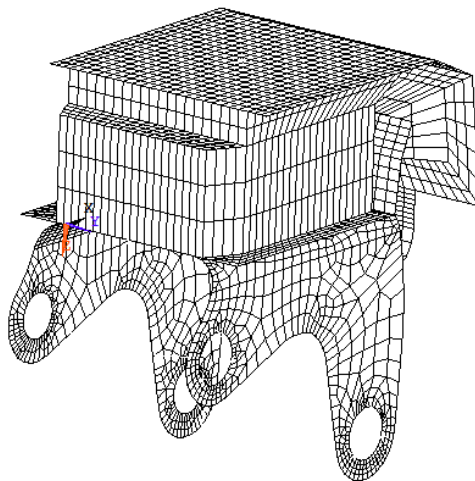

Figure 6: FE model of the sample.

3.1 Model updating of metal parts of the engine mounting

In order to ensure that any deviation between dynamic response of the sample and its FE model is due to inaccuracies in initial estimation of material constants of elastomeric region, it is necessary to model the other parts (metallic sections) correctly. It is expected that using shell elements with proper material properties, FE model can present accurate dynamic behavior of the steel brackets. Here, these material properties (elastic Young's modulus, Poisson's ratio and mass density) are ob-

tained through model updating processes. At first, the experimental FRFs of the metal parts are obtained by implementing impact hammer test. Then it is tried to identify the material properties of the components to give the best correlation between the FRFs obtained from the test and FE models. For example, the experimental and updated FE FRFs of upper bracket in z-direction are illustrated in Figure 7. The updated material properties for the brackets are presented in Table 4.

	Young' modulus [GPa]	Poisson's ratio	Mass density [kg/mm³]
Upper bracket	208	0.29	7800
Lower bracket	220	0.29	7800

Table 4: Updated material properties of the brackets.
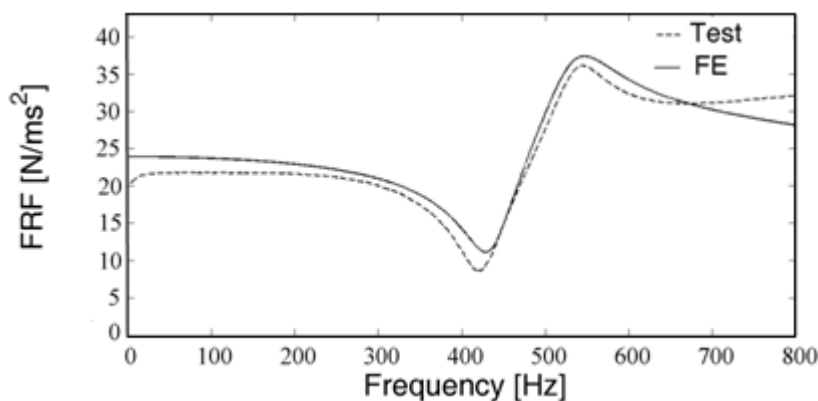

Figure 7: FRFs of updated FE model and test for upper bracket.

3.2.Mooney-Rivlin material model

Mooney–Rivlin material model that describe the rubber like materials behavior, has the variants of 2, 3, 5, and 9 terms material constants (Mooney, 1940, Rivlin, 1948). The strain energy potential function, E, of an isotropic material is customarily formulated in terms of three invariants of the stretch ratios. These are generally taken to be the principle invariants, I1, I2 and I3 of the right Cauchy-Green deformation tensor (Blatz et.al, 1973). The strain energy potential functions are usually assumed to have polynomial or reduced polynomial forms. Considering Mooney-Rivlin material models, the polynomial form for an incompressible elastomeric material can be expressed as following:

$$E = \sum_{i+j=1}^{N} Cij(I_1 - 3)^i (I_2 - 3)^j \tag{1}$$

Where

$$I_1 = \lambda_1^2 + \lambda_2^2 + \lambda_3^2$$
$$I_2 = \lambda_1^2 \lambda_2^2 + \lambda_2^2 \lambda_3^2 + \lambda_1^2 \lambda_3^2$$

λ_1 and λ_2 are the principal stretches.

For incompressible materials, it is considered that.

$$I_3 = \lambda_1^2 \lambda_2^2 \lambda_3^2 = 1$$

Depending on the value of N, different variants of Mooney-Rivlin model will be formed. For example, N=3 constructs 9-parameter Mooney-Rivlin model (the material parameters are c01, c10, c11, c02, c20, c21, c12, c30, c03) and N=1 stands for 2-parameter Mooney-Rivlin model. In later case, considering Eqn.1, the strain energy potential function is expressed as following

$$E = C_{10}(I_1 - 3) + C_{01}(I_2 - 3) \tag{2}$$

Where, c10, c01 are the material constants.

3.3 Studying the static performance of the sample

To ensure that the elastomeric engine mount is modeled correctly and the static coefficient of Mooney-Rivlin material model is estimated properly, first the static performance of the sample is investigated. The results of static analysis with together the experimental results that was achieved in section 2.2.1, are presented in Figure 8. This figure shows that the prediction of the static behavior of the component is acceptable.
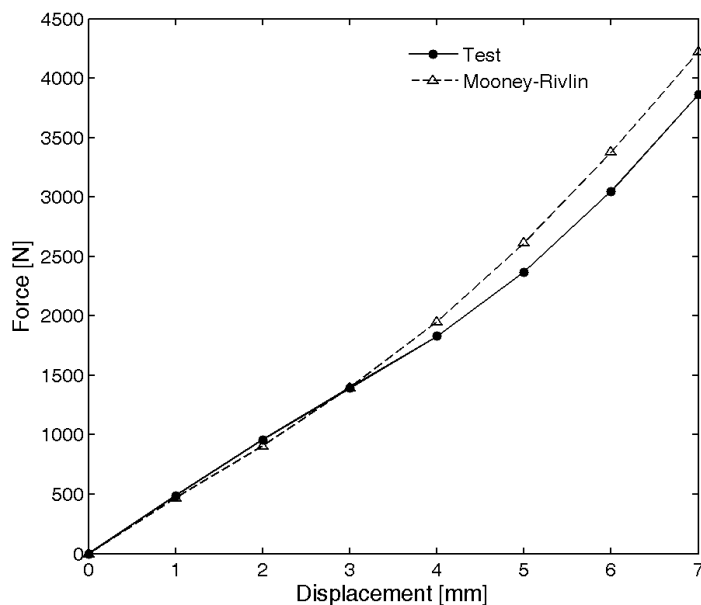

Figure 8: Comparing force-displacement curves of the static test and FE analysis for the investigated component.

4 RADIAL BASES FUNCTION NEURAL NETWORKS

For sake of the completeness, the radial basis function neural network (RBFNN) is described briefly here. Architecture of a RBFNN is shown in Figure 9. A RBFNN consist of two layers, the first containing RBF neurons and the second containing linear neurons.
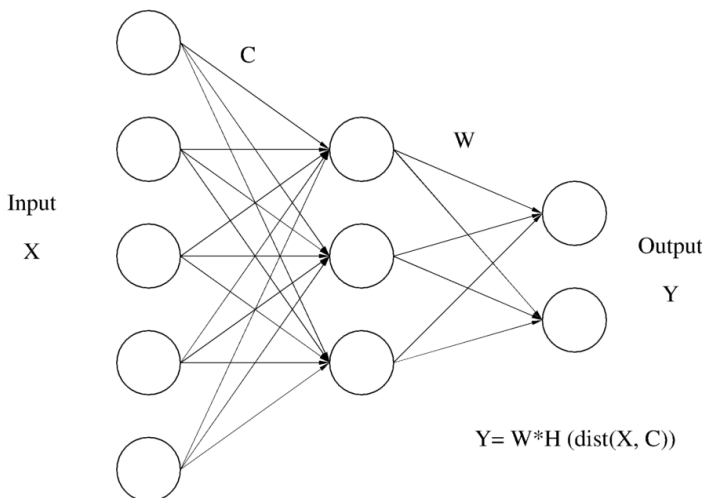
Figure 9: Architecture of a radial basis function neural network.

The overall response characteristic of an RBFN is presented in Eqn. (3) (More details can be found in (Atalla and Inman, 1998).

$$f_i = b_j + \sum_{i=1}^{n} W_{ij} \varphi(\|\{x\} - \{c_i\}\|, sc) \tag{3}$$

Where, $\{x\}$ is the value of input vector, $\{c_i\}$ is the center of the ith RBF neuron, sc is the spread constant of the network (the same for every neuron), $\| \ \|$ represents the Euclidean norm (2-norm). φ is the radial basis function of the network (the same for every neuron), f_i is the output of the jth linear neuron and w_{ij} is the weight between the ith RBF neuron and jth linear neuron and n is the number of RBF neurons.

There are two types of data that can be used for identification of dynamic characteristics of an elastomeric component, namely FRF data and Modal data. In the present work, the FRF data will be implemented.

The RBFN is trained with data obtained from solving the direct problem N times where, N is the number of training sets. To train an RBFNN, it is necessary to set every network parameter, i.e., every RBF center, all the weights and biases of the linear neuron and the spread constant. The centers of an RBFNN should be spread out over the range of the input space occupied by the input vectors. In the present work all of the input vectors are chosen as centers.

Training a RBFNN comprises the following steps:

1- The distance between each column of the input matrix X and each neuron in the hidden layer (represented by its centre c) is measured, resulting in the matrix D of distances. The element d_{ji} of this matrix is the distance between the ith column of X and the center of the jth neuron in the hidden layer.

2- The output of the hidden layer is calculated by. $h_{j,i} = e^{-d_{j,i}/sc}$ The elements of H, which measure how much the ith input vector resembles the centre of the jth neuron, range between zero and one.

3- The network output Y is calculated by a linear combination of the elements of H,

$$Y = W * H \tag{4}$$

Training a RBFNN, means finding the weight matrix W the only unknown of the problem. Solving the equation above for W yields

$$W = Y * H^+ \tag{5}$$

Where H^+ is the pseudo-inverse of H. Once it has been trained, the network can be used to estimate model parameters based on new input vectors.

4- The network generalization characteristics should be verified before implementing it. Generalization is the behavior of the network output when presented with an input vector not used to train the network.

5 IDENTIFICATION OF THE MATERIAL CONSTANTS OF THE MOONEY-RIVLIN MODEL IN LOW AMPLITUDE HIGH FREQUENCY RANGE

Here, it is tried to identify the material coefficients (c_{10}, c_{01}) using FRF data. Identification process is conducted using RBFNN. The training sets of the RBFNN consist of sensitive bands of FRFs (frequency bands around peaks) as inputs and material constants coefficients as targets. Usually, elastomers show frequency and amplitude dependent behavior and in most cases the stiffness of elastomers will increase with increasing the frequencies. So here, to generate input FRFs, the material properties are changed gradually (from the values derived from static tension test until the twice of them) as Eqn. 6.

$$c_{10} = c_{10}^0 (1 + 0.1 \times \beta) \, \& \, c_{01} = c_{01}^0 (1 + 0.1 \times \beta), \beta = 0, 1, ..., N \tag{6}$$

Where, c_{10}^0 and c_{01}^0 are the material constants that derived from static tension test.

Using each set of these material constants, transient analysis (with considering material damping coefficient) is conducted due to impulse excitation on the FE model of the investigated component. Then by doing FFT analysis, corresponding FRF graphs are derived. For instance, The FRFs resulting from three different values of β and the average FRF of the three test samples for z-direction are plotted in Figure 10 with distinct sensitive frequency bands. Fortunately considering these separate bands, it is evident that resonant frequencies show high sensitivity to material properties changes therefore, in the present work the resonant frequencies are used to training the RBFNNs in each frequency band.
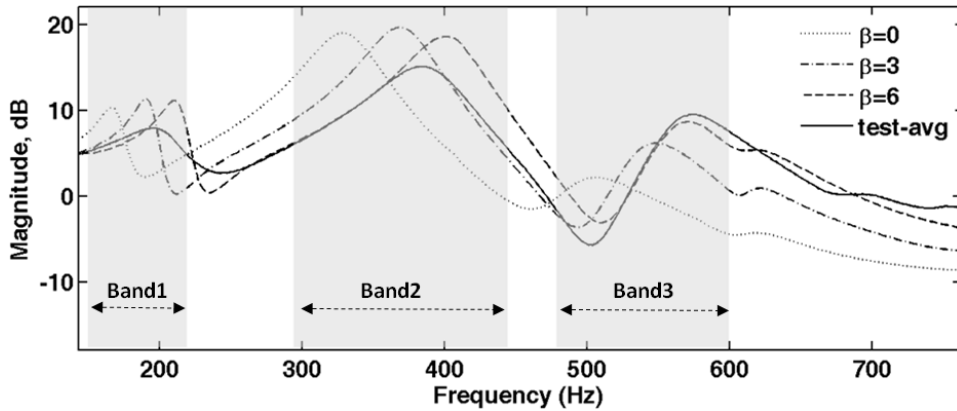
Figure 10: FRFs that are achieved from three different values of β are compared with the test counterpart.

Appropriate RBFNN for each of the frequency bands is constructed using resonant frequencies. For example training sets for the Band2 is presented in Table 5. Many points of a FRF graphs in each frequency band can be used in identification process using artificial neural networks. Even though this strategy may lead to more accurate identified values however, it also needs many training sets. Location of Table 5.

After training the corresponding RBFNN of a specified frequency band, the measured frequency response function (here the resonant frequency) in the same frequency band is fed to the network and value of corresponding β is determined. Then using equation 6, the material constants of the 2-parameter Mooney-Rivlin model, namely c_{10} and c_{01}, are identified. The flowchart of the identification process is illustrated in Figure 11. The predicted material constants using this procedure for the investigated engine mount is presented in Figure 12. Also using these predicted material constants in z-direction, the stress-strain curves at different frequencies are plotted in Figure 13. Considering these results, it is evident that the elastomeric component shows frequency dependent behavior and also, there is deviation from isotropic assumption in a real elastomeric component.

Training set / No.	1	2	3	4
Input: Resonant frequency	{ 328	{ 369	{ 391	{ 402
Target: β	0	3	5	6

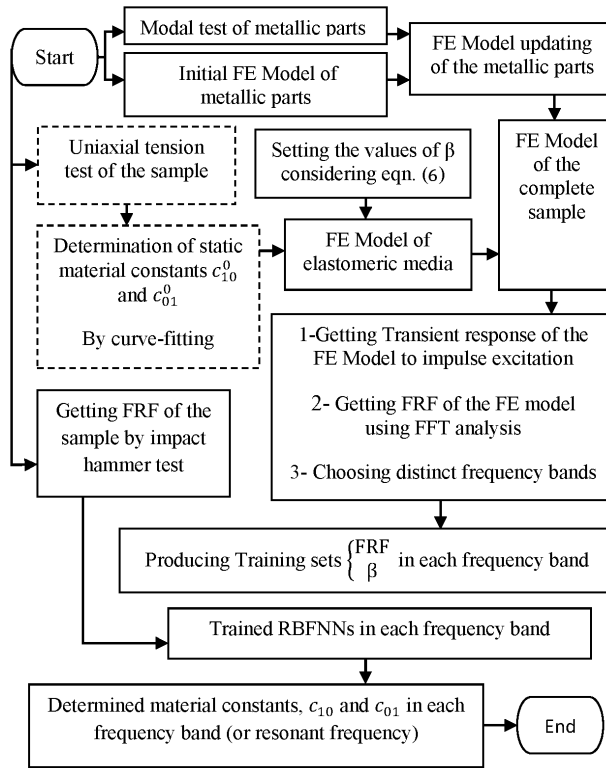**Table 5:** Training set for Band2 in z-direction.

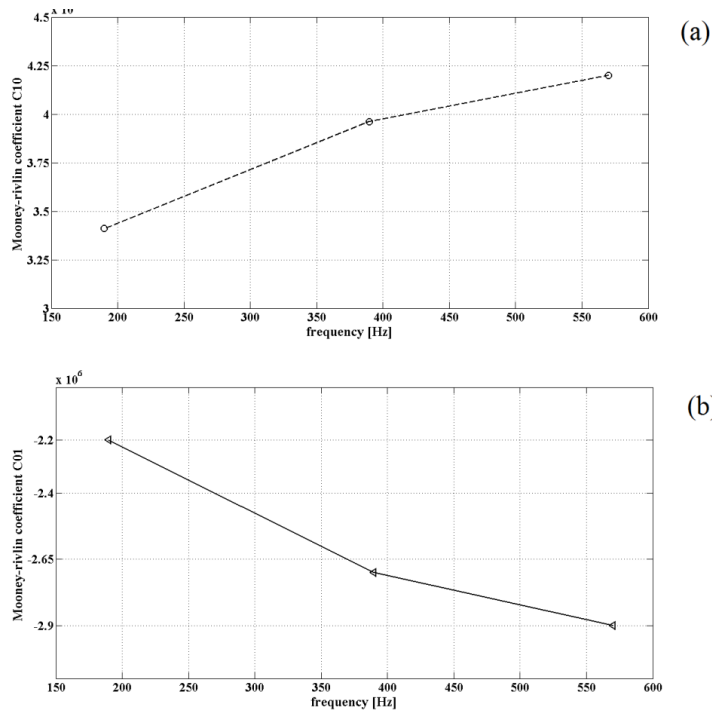**Figure 11:** Flowchart of the identification procedure.

Figure 12: Predicted material constants of the 2-parameter Mooney-Rivlin model for elastomeric media of the elastomer-ic engine mount _ _ _ _ _ _ _ c_{10} ;-------- c_{01}
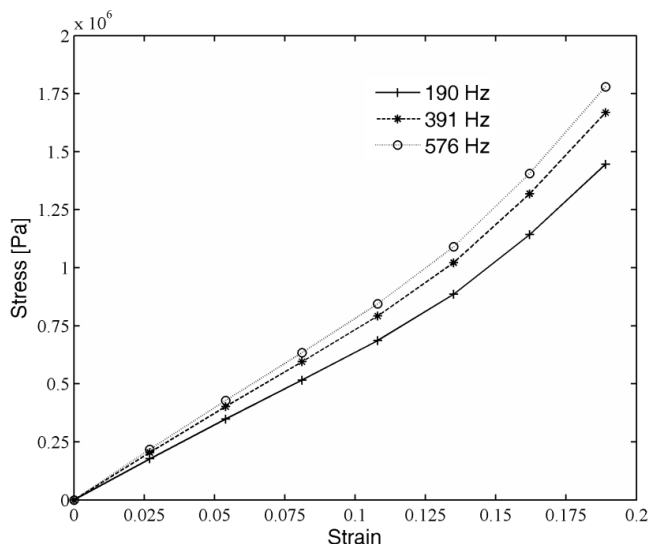
Figure 13: Stress-strain diagram at different frequencies in z- direction for the investigated engine mount.

6 IDENTIFICATION OF THE MATERIAL CONSTANTS OF THE MOONEY-RIVLIN MODEL IN HIGH AMPLITUDE LOW FREQUENCY RANGE

Here, in order to investigate the effect of deflection amplitude on the coefficients of 2-parameter Mooney-Rivlin model, a new test setup is implemented in low frequency range. This test setup is shown in Figure 13. In current setup, different weights (namely with masses of 2.5, 7.5 and 25 kg) are added on the top of engine mount and the mount is fixed from the bottom brackets to a heavy rigid block. It is obvious that this kind of boundary condition allows moderate deflection of the sample comparing to the low deflection in Free-Free condition. Addition of weight on the sample extremely reduces the natural frequencies of the system. For instance, time response on the top of the engine mount using 2.5Kg weight is presented in Figure 14.

Identification process was carried out similar to high frequency state using neural network (RBFNN). Similar to previous section, natural frequencies were used as target in FBFNN. The predicted coefficients of 2-parameter Mooney-Rivlin model (using the natural frequencies of bounce mode with different added weights where the deflection of elastomeric media is in upward and downward) are compared with low amplitude high frequency results in Figures 15 and 16. These results show that the material constants of elastomeric media depend not only to the frequency of excitation but also to the amplitude of the deflections. The magnitudes of identified values for material constants in both dynamic low and high amplitude cases are greater than the static test results.
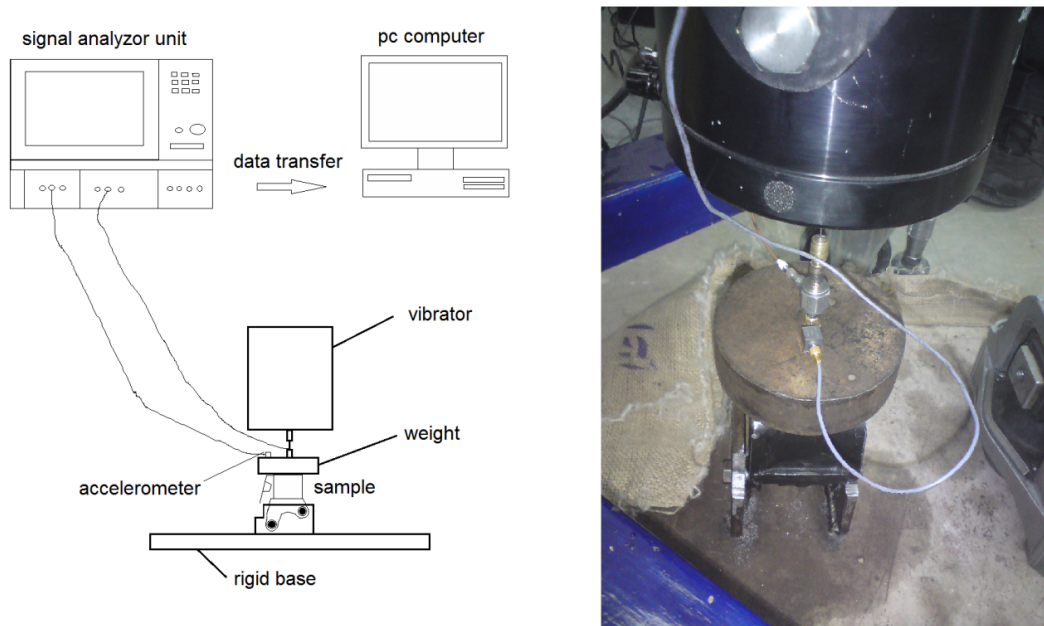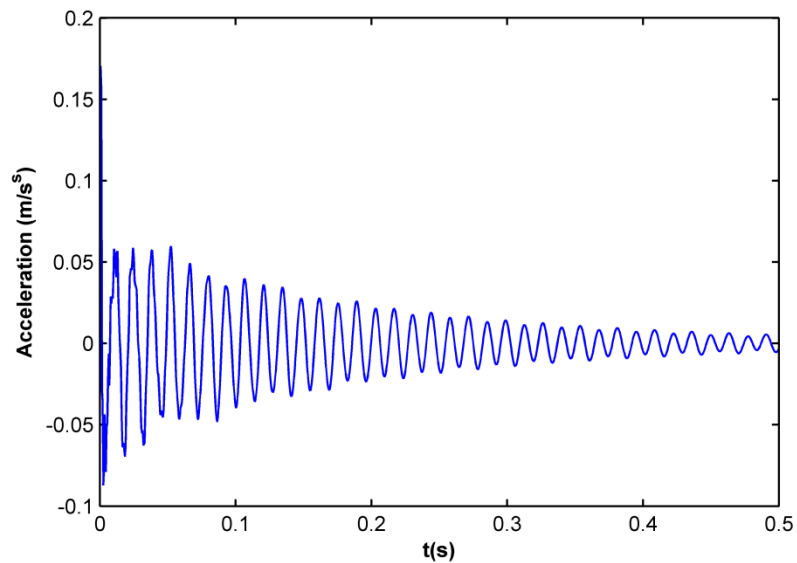
Figure 13: Low-Frequency test setup.

Figure 14: Time response on the top of the engine mount using 2.5Kg weight.

Figure 15: Predicted material constants of the 2-parameter Mooney-Rivlin model for elastomeric media of the elastomeric engine mount, c_{10} in: _ _ _ _ _ _ low-frequency range and - - - - High-frequency range.
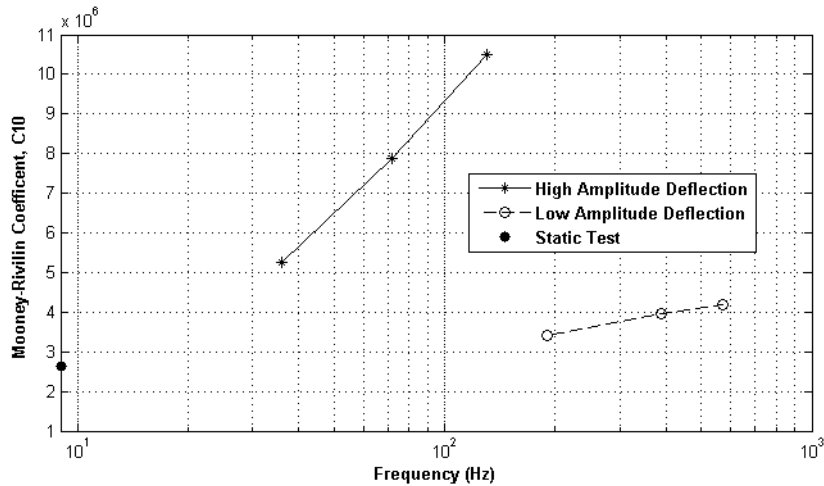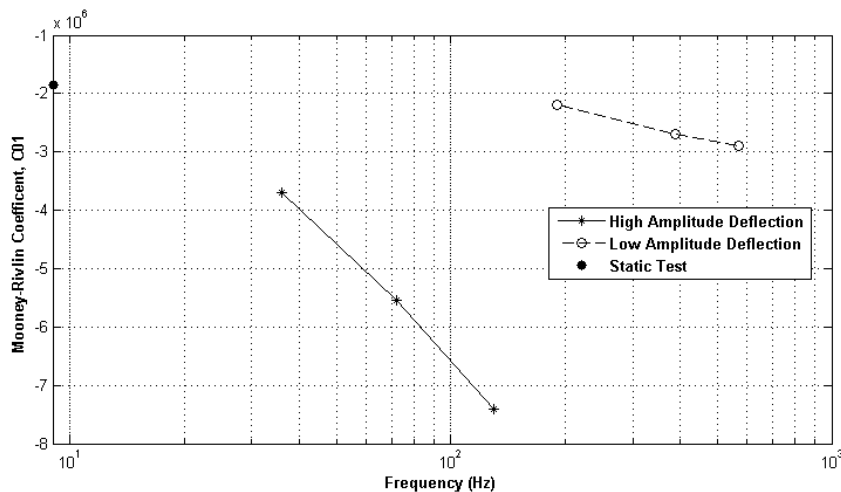

Figure 16: Predicted material constants of the 2-parameter Mooney-Rivlin model for elastomeric media of the elastomeric engine mount, c_{01} in: _ _ _ _ _ _ low-frequency range and - - - - High-frequency range.

7 CONCLUSION

In the present work, a procedure to determine the broad band frequency dependent material constants of 2-parameter Mooney-Rivlin model for elastomeric components (here, the elastomeric engine mount) was developed. It is found that Radial Basis Function Neural Network and banded FRF data can be used successfully in prediction process on real components. The results showed that in dimensionally compact elastomeric components, instead of using many points of the banded FRF graph and natural frequency in training the networks, the only natural frequency can lead to acceptable results. The results showed that the Mooney Rivlin material constants for incompressible elastomeric components are frequency and deflection amplitude dependent. Finally, the proposed

procedure is general and can be applied to identify dynamic material constants of the other constitutive models such as Ogden, Neo-Hookean, etc for elastomers.

References

Atalla, M.J, Inman, D.J. (1998). On Model Updating Using Neural Networks. Mechanical Systems and Signal Processing.

 12: 135-161.

Blatz, P.J., Sharda, S.C., Tschoegl, N.W. (1973). A new elastic potential function for rubbery material. Proceedings of the National Academy of Sciences of the United States of America 70: 3041–3042.

Christopherson, J., Jazar, G.N. (2006). Dynamic behavior comparison of passive hydraulic engine mounts: Part 2Finite element analysis. Journal of Sound and Vibration 290: 1071-1090.

Guo Z., Sluys, L.J. (2006). Application of a new constitutive model for the description of rubber-like materials under monotonic loading. International Journal of Solids and Structures 43:2799-2819.

Gupta, A., Khandaswamy, S., Yellepeddi, S., Mulcahy, T., Hull, J. (1999). Dynamic modulus estimation and structural vibration analysis. Proceedings of the 17th International Modal Analysis Conference, Kissimmee FL(UA) Proc SPIE 3727: 1423–1427.

Hofer,P. ,Lion, A. (2009). Modelling of frequency- and amplitude-dependent material properties of filler-reinforced rubber. Journal of the Mechanics and Physics of Solids 57:500-520.

Jahani, K., Nobari, A.S. (2010). Identification of damping and dynamic young's modulus of a structural adhesive using radial basis function neural networks and modal data. Experimental Mechanics 50:607–619.

Khalilollahi, A, Felker, B.P., Wetzel, J.W. (2002). Non-linear elastomeric spring design using Mooney-Rivlin constants, Proceedings of 2002 ANSYS Users Conference and Exhibition, Paper.146.

Kim, B.K., Youn, S.K., Lee, W.S. (2004). A constitutive model and FEA of rubber under small oscillatory load superimposed on large static deformation, Archive of Applied Mechanics 73:781–798.

Korochkina, T.V., Jewell, E.H., Claypole, T.C., Gethin, D.T. (2008). Experimental and numerical investigation into nonlinear deformation of silicone rubber pads during ink transfer process, Polymer Testing 27 : 778-791.

Mooney, M. (1940). A theory of large elastic deformation, Journal of Applied Physics 11:582-592.

Pearson, I, Pickering, M. (2001).The determination of a highly elastic adhesive's material properties and their representation in finite element analysis, Finite Elements in Analysis and Design 37: 221-232.

Pereira, C.E.L. and Bittencourt, M.L. (2010). Topological sensitivity analysis for a two-parameter Mooney-Rivlin hyperelastic constitutive model, Latin American Journal of Solids and Structures 7:391-411.

Rendek, M., Lion, A. (2010). Amplitude dependence of filler-reinforced rubber: Experiments, constitutive modelling and FEM – Implementation, International Journal of Solids and Structures 47: 2918–2936.

Rivlin, R.S. (1948). Large elastic deformations of isotropic materials. IV. Further developments of the general theory, Philosophical Transactions A 241:379-397.

Silva, C.A.C. and Bittencourt, M.L. (2008). Structural shape optimization of 3D nearly-incompressible hyperelasticity problems, Latin American Journal of Solids and Structures 5:129-156.

Wismer, N.J., Gade, S. (1997). Improved method for complex modulus estimation, B&K Application note. pp.1-7.